Appendix A: CH_3CO^+ in other sources

The acetyl cation, CH_3CO^+, has also been detected towards L483, L1544, and L1527 (see Fig. A.1). However, it is not observed towards Sgr B2 (PRIMOS [3] line survey; Neill et al. 2012), towards Orion-KL (Tercero et al. 2010, 2011), or in our line survey of B1 (Marcelino et al. 2007, 2009, 2010; Cernicharo 2012). In the PRIMOS data on SgrB2, a very tentative detection of the J=1-0 K=0 line could be claimed at a velocity of 80 km s^{-1}. However, only an upper limit can be obtained for the J=2-1 transition as this line is heavily blended with a strong line of acetone. It seems, hence, that CH_3CO^+ is typical of cold interstellar clouds.

Appendix B: Potential carriers of the series of lines

All known diatomic species in cold dark clouds have overly large rotational constants compared with those derived from the lines in TMC-1. For example, a molecule containing one S (CS, NS, SO) will have a rotational constant that is too high by more than 12 GHz. Adding one or two H atoms to these combinations of sulphur produces radicals (with overly high rotational constants, such as HCS) or asymmetric rotors such as H_2CS, which is too heavy (Müller et al. 2019). A molecule with two S atoms is, of course, too heavy (for example, $B(S_2)$=8831 MHz; Pickett 1979), and we do not expect to have Si- or P-bearing polyatomic species in this cloud. The first step in finding candidates is to exclude the possibility of having a slightly asymmetric species. In that case, we could expect to have lines corresponding to K=±1 at roughly ±(B-C) from the K=0 lines. We searched in the Q-band survey (J=2-1) for such a pattern. No lines up to one-fourth of the intensity of the K=0 line are observed. Moreover, taking into account that there is no evidence for a radical as a possible carrier, the species resulting from the addition of one hydrogen to the closed-shell asymmetric species HNCO, HCOOH, and H_2CCC have to be excluded. However, their protonated species are also, at least in principle, closed-shell species. Hence, possible candidates are H_2CCCH^+, $CH_3CCH_2^+$, $HCNOH^+$, $HNCOH^+$, $HCOOH_2^+$, and CH_3OO^+, all of which, with the exception of the last one, are protonated forms of known neutral and abundant species in TMC-1. Nevertheless, the resulting molecular structures will be highly asymmetric for most of them, or they are too light or too heavy, as are the cases for H_2CCCH^+ and $CH_3CCH_2^+$, respectively. $HNCOH^+$ is a linear species characterized in the laboratory with a rotational constant of 9955 MHz (Latanzi et al. 2012) and is not detected in our data. Other exotic species, such as NH_2CHOH^+, $CH_2ONH_2^+$, and CH_3NOH^+, which could result from the protonation of interesting molecules (NH_2CHO for example), are discarded for their molecular asymmetry and because the neutral species have not been observed in TMC-1. Ab initio calculations have been performed for the most promising candidates (see Table B.1), and their isomers and the results are discussed in Sect. 3.1.

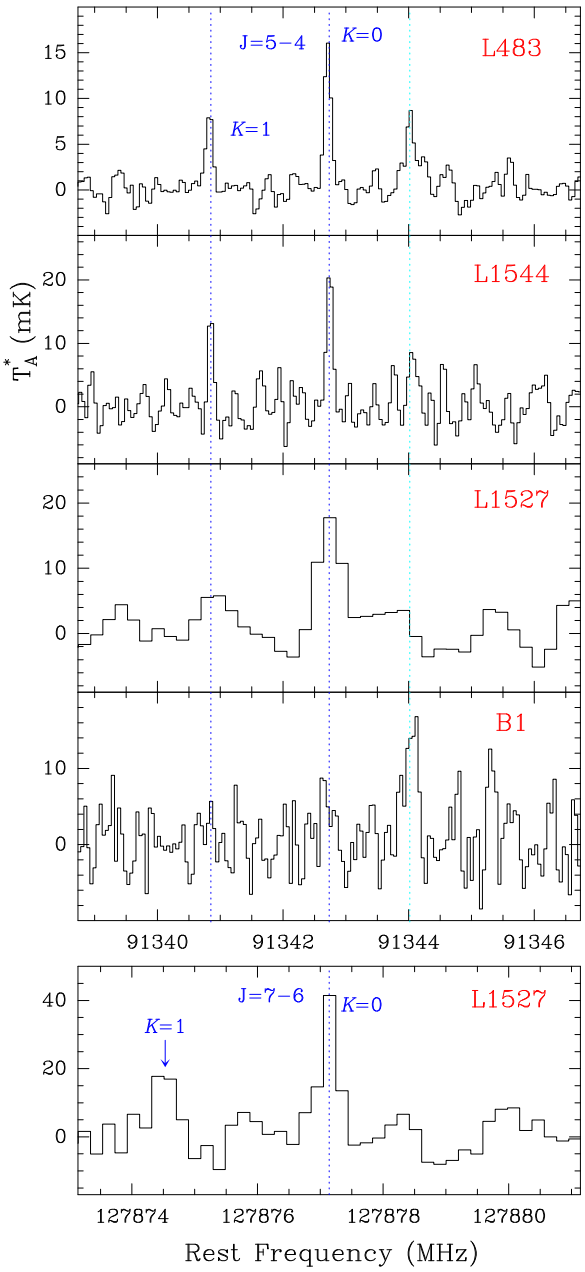

Fig. A.1. Observations of the J=5-4 transition of CH_3CO^+ towards L483, L1544, L1527, and B1 (top panels); the bottom panel shows the J=7-6 line towards L1527. The abscissa corresponds to the rest frequency (in MHz) and the ordinate is the antenna temperature (in mK). The spectral resolution is 48.8 kHz for all sources except L1527, for which it is 198 kHz. The vertical dashed blue lines indicate the position of the K = 0 and K = 1 lines (detected in all sources except B1), and the cyan line corresponds to the U feature at 91344 MHz (detected in all sources except L1527). The rest velocities of L1527 and L1544 were taken as v_{LSR}= 5.9 km/s and 7.2 km/s, respectively, based on Sakai et al. (2009) and Vastel et al. (2015), respectively.

Appendix C: Additional quantum chemical calculations for CH_3CO^+

The potential energy surface (PES) for the protonation of ketene has been explored at the CCSD/cc-pVTZ level of theory. In the calculations, we considered three possible proton donors: H_3^+, H_3O^+, and HCO^+, as well as the formation of the two isomers of protonated ketene, CH_3CO^+ and CH_2COH^+. Figure C.1 depicts the PES along the reaction coordinate for the protonation of ketene and the relative energies for all the stationary points when ketene reacts with H_3^+, H_3O^+, or HCO^+. For each reaction, the two reactants, ketene and the proton donor, that separated from each other were assumed to be the energy zero. The protonation

[3] Access to the entire PRIMOS data set, specifics on the observing strategy, and overall frequency coverage information is available at http://www.cv.nrao.edu/~aremijan/PRIMOS/

Table B.1. Rotational constants and electric dipole moments of potential candidates.

Species[a]	ΔE/kJ/mol[b]	A, B, C/MHz	D_J, D_{JK}/kHz	μ_a, μ_b, μ_c/D
		154355.3	3.9	2.5
	0.0	9107.2	178.7	0.0
H_3CCO^+		9107.2		0.0
		201325.3	2.7	1.6
	178.0	9411.2	341.6	0.1
H_2COH^+		9222.3		0.0
		155571.2	3.8	1.9
	0.0	9090.7	160.6	0.0
H_3CNCH^+		9090.7		0.0
		285625.5	2.6	0.5
	0.0	9673.5	457.3	0.0
H_2CCCH^+		9356.6		0.0
		280905.8	3.5	5.0
	0.0	10338.2	492.0	0.0
H_2CCN^+		9971.2		0.0
		277331.4	4.00	3.7
	5.9	11582.1	685.4	0.0
H_2CNC^+		11117.8		0.0
		595150.6	2.7	1.5
	102.5	10359.3	1285.8	1.9
$HNCCH^+$		10182.1		0.0
		328396.0	3.6	4.6
	176.4	10180.7	593.3	0.0
H_2NCC^+		9874.5		0.0
	196.2	11120.9	2.9	0.0
$HCNCH^+$				
		324210.9	2.9	3.8
	0.0	10295.5	380.4	0.0
H_2NCO^+		9978.6		0.0
		723374.4	2.8	1.3
	70.4	10034.0	1255.3	1.7
$HNCOH^+$		9896.7		0.0
		625942.1	3.8	2.4
	285.4	10400.0	1859.1	1.6
$HCNOH^+$		10230.0		0.0
		268002.3	3.6	2.9
	333.8	11140.1	461.1	0.0
H_2CNO^+		10695.5		0.0
		259994.7	4.6	2.3
	613.2	11321.2	484.7	0.0
H_2CON^+		10848.8		0.0

Notes. [a] Calculations at the CCSD/cc-pVTZ level of theory. [b] The energy taken as reference is the lowest energy species within the same isomer family .

of ketene in the CH_2 in the three cases is exothermic, and it proceeds without any transition state (TS) to form CH_3CO^+. This formation is more favourable in the case of H_3^+. On the other hand, the formation of CH_2COH^+ is exothermic in the cases of H_3^+ and HCO^+, but endothermic in the case of H_3O^+. The less stable isomer, CH_2COH^+, can interconvert through a hydrogen migration to CH_3CO^+, which has a TS barrier height of 210.1 kJ/mol. As shown in Figure C.1, the TS for this interconversion lies over the energy of the reactants in the protonation of ketene with H_3O^+ and HCO^+. In contrast, this TS lies below the energy of the reactants when ketene reacts with H_3^+.

Appendix D: CH_3X species in TMC-1

As noted above, the intensity of the J=2-1 K=1 line in TMC-1 is well below the expected value if the rotational temperature for the A and E species is the same. In order to check this point, we show in Fig. D.1 the rotational diagrams for the A and E species of CH_3CO^+ using the observed line parameters given in Table 1. The observed intensities have been corrected for beam dilution and the beam efficiencies of the Yebes 40m and IRAM 30m telescopes. We assumed a uniform source of radius 40″ (Fossé et al. 2001). The derived rotational temperatures, $T_{rot}(A)$=4.4±0.4 K and $T_{rot}(E)$=5.0±0.5 K, are consistent with a common excitation through collisions with H_2. The de-

Table B.2. Scaled theoretical values for the spectroscopic parameters of CH_3CO^+, CH_2COH^+, and CH_3NCH^+ (all in MHz).

	CH_3CN		CH_3CO^+		
Parameter	Calc.[a]	Exp.[b]	Calc.[a]	Scaled[c]	Exp.[d]
$(A\text{-}B)\times10^{-3}$	150.4	148.900074(65)	145.0	143.5	-
B	9191.5	9198.899134(11)	9122.3	9129.6	9134.4742(8)
$D_J\times10^3$	3.6	3.807528(9)	3.7	3.9	4.014(13)
$D_{JK}\times10^3$	174.0	177.40796(28)	181.0	184.6	188.47(50)
	CH_2CNH		CH_2COH^+		
Parameter	Calc.[a]	Exp.[e]	Calc.[a]	Scaled[f]	Exp.[d]
A	198393.1	201443.685(75)	198278.8	201327.7	-
B	9666.3	9663.168(2)	9411.8	9408.7	-
C	9488.0	9470.127(2)	9227.6	9210.2	9134.4742(8)
$D_J\times10^3$	2.9	2.980(2)	2.7	2.8	4.014(13)
$D_{JK}\times10^3$	244.4	232.8(3)	397.7	378.7	188.47(50)
	CH_3NC		CH_3NCH^+		
Parameter	Calc.[a]	Exp.[g]	Calc.[a]	Scaled[h]	Exp.[d]
$(A\text{-}B)\times10^{-3}$	169.0	167.36100(23)	164.5	162.9	-
B	10049.0	10052.88568(25)	9102.0	9105.5	9134.4742(8)
$D_J\times10^3$	4.4	4.69212(18)	3.8	4.0	4.014(13)
$D_{JK}\times10^3$	222.9	227.5116(83)	168.2	171.7	188.47(50)

Notes. [(a)] Rotational constants calculated at the CCSD(T)-F12b/aug-cc-pVQZ level of theory, and centrifugal distortion constants calculated at the MP2/aug-cc-pVQZ level of theory. [(b)] Müller et al. (2009). [(c)] Scaled by the ratio Exp/Calc. of the corresponding parameter for CH_3CN species . [(d)] This work. [(e)] Rodler et al. (1984). [(f)] Scaled by the ratio Exp/Calc. of the corresponding parameter for CH_2CNH species . [(g)] Plíva et al. (1995). [(h)] Scaled by the ratio Exp/Calc. of the corresponding parameter for CH_3NC species .

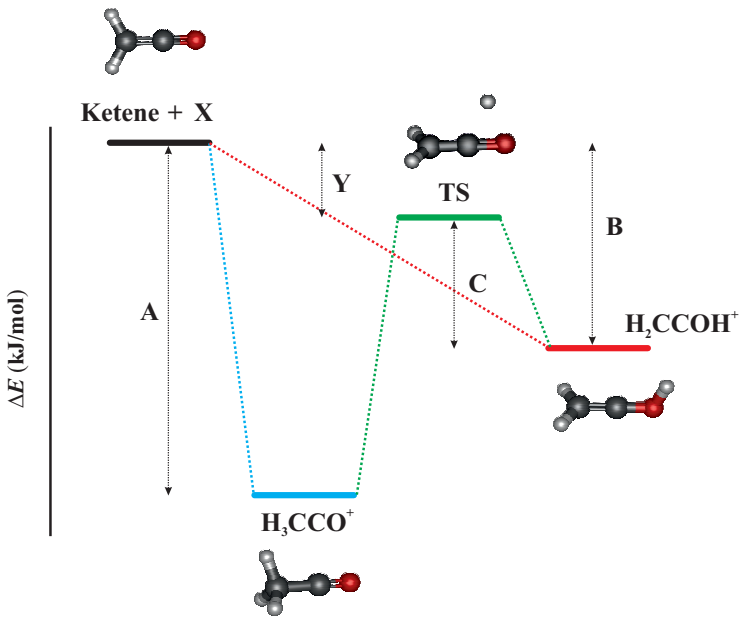

	X=H_3^+	X=H_3O^+	X=HCO^+
A	-421.8	-130.9	-244.8
B	-241.1	49.8	-64.1
C*	210.1	210.1	210.1
Y**	-31.0	259.9	146.0

Fig. C.1. Energy diagram for the protonation of ketene. Total energies relative to those of the separated reactants, ketene and the proton donor X, are given in the enclosed table in kJ mol^{-1}. C* is the TS energy for the interconversion between CH_2COH^+ and CH_3CO^+ isomers. Y** is the energy difference between the reactants and the interconversion TS; a negative value indicates that the TS is submerged below the reactant energy, and a positive value implies that the TS lies above the reactant energy.

rived column densities are N(A-CH_3CO^+)=(2.2±0.2)×10^{11} cm^{-2} and N(E-CH_3CO^+)=(9.7±0.9)×10^{10} cm^{-2}. Hence, as discussed in Sect. 3.4, the A/E abundance ratio for CH_3CO^+ has been modified through collisions with H^+, H_3^+, HCO^+, and H_3O^+. This is a similar effect to that found in cold molecular clouds for molecules having ortho and para symmetry species.

In order to check this peculiar result, we analysed all symmetric rotors having transitions within our line survey: CH_3CCH, CH_3C_4H, CH_3CN, and CH_3NC. The cation CH_3CNH^+ has not been detected in TMC-1 (see Sect. 3.3). The symmetric top CH_3C_3N is discussed in Marcelino et al. (2020b). Figure D.2 shows the J=2-1 transition for CH_3CN, CH_3CCH, CH_3NC, and CH_3CO^+ (for this species, see also Fig. 1). The K=0 and K=1 lines of CH_3CN exhibit the typical hyperfine structure introduced by the quadruple moment of the N nucleus. For all these additional molecules, we assumed a rotational tem-

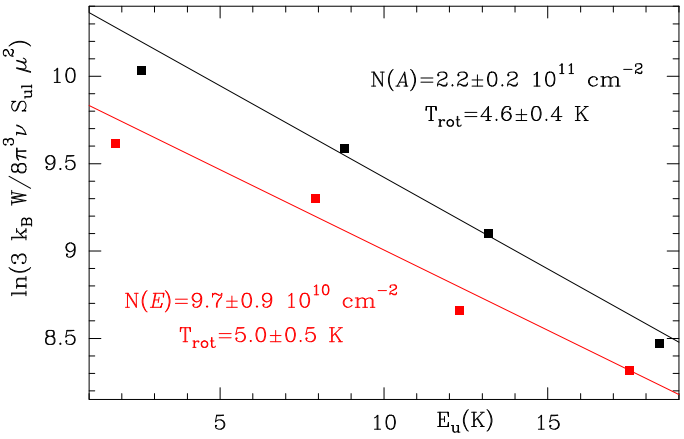

Fig. D.1. Rotational diagrams for the A (black line) and E (red line) symmetry species of CH_3CO^+ in TMC-1.

perature of 10 K and a source radius of 40″ (Fossé et al. 2001), and we produced a synthetic spectrum that is compared to the observations. We found that the A/E abundance ratio is $\simeq$1 for all species but CH_3CO^+. Adopting a lower rotational temperature has little effect on the derived A/E abundance ratio for these symmetric rotors.

Appendix E: Observed and calculated frequencies of CH_3CO^+

The frequencies observed in space and in the laboratory were merged to obtain the recommended rotational and distortion constants. A total of 89 rotational transitions, ten in space (see Table 1) and 79 in the laboratory (see Table E.1), were fitted to the standard Hamiltonian of a symmetric rotor (Gordy & Cook 1984). For the lines observed in TMC-1 and other dark clouds, only B, D_J, and D_{JK} can be obtained as only rotational transitions with K=0 and 1 have been observed. The results are given in Table 2. For the 79 lines observed in the laboratory, the constants H_{JK} and H_{KJ} were included in the fit, and the results are given in Table 2. Finally, the merged fit to the astronomical and laboratory lines produces the recommended set of rotational constants given in the last column of Table 2. The observed and calculated frequencies, together with the observed minus calculated values for the merged fit, are given in Table E.1.

We used the rotational and distortion constants that resulted from the merged fit to the astronomical and laboratory lines (see Table 2) to produce frequency predictions, frequency uncertainties, line strengths, upper energy levels, and Einstein coefficients for all transitions involving levels with energies below 2000 K. They are given in Table E.2. The whole table is electronically available at the CDS. It should be noted that this table contains the transitions for the A and E species, and that the E lowest energy level, J_K=1_1, is 7.8 K above the 0_0 level of the A species.

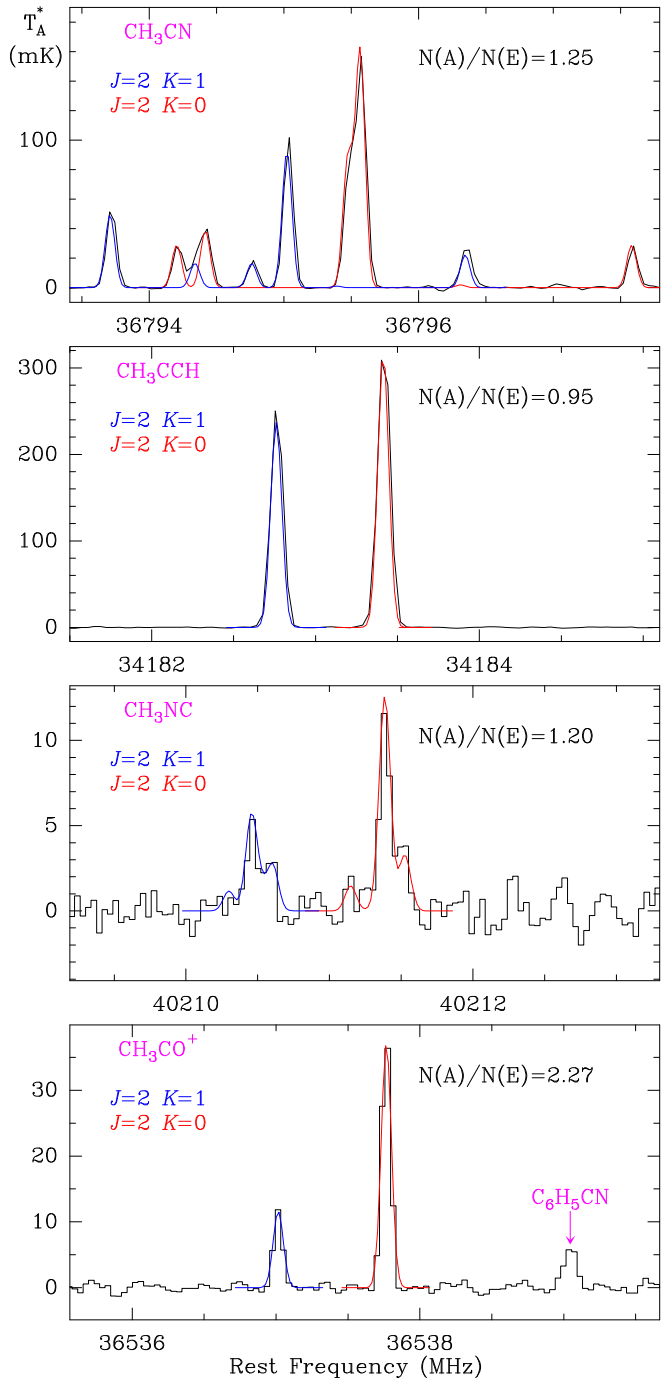

Fig. D.2. Observed lines in the transition J=2-1 K=0,1 of different symmetric rotors in TMC-1. The colour lines represent the expected line profiles for the A species (red) and E species (blue). The abundance ratio between them in the model is indicated in each panel.

Table E.1. Observed and calculated frequencies (in MHz) for CH_3CO^+.

J_u	K	Freq. Obser.	(Unc)	Freq. Calc.	(Unc)	Obs-Calc
2	0	36537.765	0.010	36537.761	0.001	0.004
2	1	36537.014	0.010	36537.010	0.001	0.004
4	0	73074.769	0.010	73074.755	0.002	0.014
4	1	73073.252	0.010	73073.253	0.002	-0.001
5	0	91342.732	0.010	91342.725	0.003	0.007
5	1	91340.865	0.010	91340.848	0.003	0.017
6	0	109610.225	0.010	109610.215	0.003	0.010
6	1	109607.954	0.010	109607.963	0.003	-0.009
7	0	127877.133	0.025	127877.131	0.004	0.002
7	1	127874.494	0.050	127874.504	0.004	-0.010
10	3	182639.714	0.050	182639.724	0.011	-0.010
10	2	182658.451	0.050	182658.469	0.006	-0.018
10	1	182669.687	0.050	182669.719	0.005	-0.032
10	0	182673.442	0.050	182673.470	0.005	-0.028
11	3	200900.043	0.050	200900.014	0.012	0.029
11	2	200920.617	0.050	200920.630	0.007	-0.013
11	1	200933.010	0.050	200933.002	0.006	0.008
11	0	200937.148	0.050	200937.127	0.006	0.021
12	3	219159.236	0.050	219159.253	0.013	-0.017
12	2	219181.747	0.050	219181.737	0.008	0.010
12	1	219195.209	0.050	219195.232	0.006	-0.023
12	0	219199.712	0.050	219199.731	0.006	-0.019
13	3	237417.332	0.050	237417.345	0.014	-0.013
13	2	237441.706	0.050	237441.696	0.008	0.010
13	1	237456.320	0.050	237456.311	0.007	0.009
13	0	237461.178	0.050	237461.184	0.007	-0.006
14	3	255674.171	0.050	255674.193	0.015	-0.022
14	2	255700.388	0.050	255700.410	0.009	-0.022
14	1	255716.107	0.050	255716.145	0.007	-0.038
14	0	255721.370	0.050	255721.391	0.007	-0.021
16	3	292183.778	0.050	292183.777	0.017	0.001
16	2	292213.646	0.050	292213.722	0.010	-0.075
16	1	292231.636	0.050	292231.694	0.008	-0.058
16	0	292237.659	0.050	292237.685	0.008	-0.026
17	3	310436.291	0.050	310436.322	0.019	-0.031
17	2	310468.201	0.100	310468.127	0.011	0.074
17	1	310487.210	0.050	310487.216	0.009	-0.006
17	0	310493.523	0.050	310493.580	0.009	-0.057
18	3	328687.226	0.050	328687.241	0.020	-0.015
18	2	328720.866	0.050	328720.905	0.012	-0.039
18	1	328741.056	0.050	328741.110	0.010	-0.054
18	0	328747.827	0.050	328747.846	0.010	-0.019
21	6	383217.758	0.050	383217.721	0.096	0.037
21	5	383303.931	0.050	383303.862	0.064	0.069
21	4	383374.395	0.050	383374.396	0.041	-0.001
21	3	383429.306	0.050	383429.289	0.025	0.017
21	2	383468.517	0.050	383468.517	0.015	0.000
21	1	383492.044	0.050	383492.060	0.012	-0.016
21	0	383499.892	0.050	383499.910	0.012	-0.018
22	6	401451.192	0.050	401451.205	0.103	-0.013
22	5	401541.411	0.050	401541.408	0.069	0.003
22	4	401615.264	0.050	401615.268	0.044	-0.004
22	3	401672.742	0.050	401672.750	0.027	-0.008
22	2	401713.849	0.050	401713.827	0.017	0.022
22	1	401738.482	0.050	401738.481	0.014	0.001
22	0	401746.707	0.050	401746.700	0.014	0.007
23	6	419682.601	0.050	419682.598	0.111	0.003
23	5	419776.829	0.050	419776.858	0.074	-0.029
23	4	419854.065	0.050	419854.039	0.048	0.026
23	3	419914.100	0.050	419914.106	0.029	-0.006

Table E.1. continued.

J_u	K	Freq. Obser.	(Unc)	Freq. Calc.	(Unc)	Obs-Calc
23	2	419957.037	0.050	419957.031	0.018	0.006
23	1	419982.794	0.050	419982.794	0.015	0.000
23	0	419991.387	0.050	419991.383	0.015	0.004
24	6	437911.779	0.050	437911.807	0.119	-0.026
24	5	438010.092	0.050	438010.117	0.080	-0.025
24	4	438090.613	0.050	438090.615	0.052	-0.002
24	3	438153.261	0.050	438153.263	0.032	-0.002
24	2	438198.039	0.050	438198.033	0.020	0.006
24	1	438224.913	0.050	438224.903	0.016	0.010
24	0	438233.877	0.050	438233.861	0.016	0.016
25	6	456138.764	0.150	456138.735	0.129	0.029
25	5	456240.963	0.150	456241.090	0.087	-0.127
25	4	456324.889	0.050	456324.900	0.056	-0.011
25	3	456390.167	0.050	456390.126	0.034	0.041
25	2	456436.758	0.050	456436.737	0.022	0.021
25	1	456464.703	0.050	456464.712	0.018	-0.009
25	0	456474.048	0.050	456474.039	0.018	0.009
26	5	474469.660	0.050	474469.681	0.094	-0.021
26	4	474556.835	0.050	474556.798	0.061	0.037
26	3	474624.604	0.050	474624.597	0.037	0.007
26	2	474673.034	0.050	474673.048	0.024	-0.014
26	1	474702.158	0.050	474702.127	0.020	0.031
26	0	474711.811	0.050	474711.821	0.020	-0.010
27	5	492695.931	0.150	492695.796	0.102	0.135
27	4	492786.129	0.150	492786.214	0.066	-0.085
27	3	492856.584	0.050	492856.582	0.041	0.002
27	2	492906.862	0.050	492906.869	0.026	-0.007
27	1	492937.060	0.050	492937.050	0.022	0.010
27	0	492947.117	0.050	492947.112	0.022	0.005

Table E.2. Frequency predictions for CH_3CO^+ *.

J_u[a]	K_u[a]	J_l[a]	K_l[a]	ν(MHz)[b]	Unc(MHz)[c]	E_{up}(K)[d]	A_{ij}(s^{-1})[e]	S_{ij}[f]	g_u[g]
1	0	0	0	18268.92826	0.00039	0.9	2.898×10^{-07}	1.0000	3
2	1	1	1	36537.00979	0.00072	9.5	2.086×10^{-06}	1.5000	5
2	0	1	0	36537.76068	0.00079	2.6	2.782×10^{-06}	2.0000	5
3	2	2	2	54801.89688	0.00115	32.8	5.587×10^{-06}	1.6667	7
3	1	2	1	54805.27517	0.00107	12.1	8.941×10^{-06}	2.6667	7
3	0	2	0	54806.40143	0.00117	5.3	1.006×10^{-05}	3.0000	7
4	3	3	3	73061.24457	0.00265	70.7	1.081×10^{-05}	3.5000	18
4	2	3	2	73068.74904	0.00151	36.3	1.854×10^{-05}	3.0000	9
4	1	3	1	73073.25310	0.00141	15.7	2.318×10^{-05}	3.7500	9
4	0	3	0	73074.75469	0.00154	8.8	2.473×10^{-05}	4.0000	9
5	4	4	4	91312.71293	0.00563	123.3	1.776×10^{-05}	1.8000	11
5	3	4	3	91325.83851	0.00326	75.1	3.159×10^{-05}	6.4000	22
5	2	4	2	91335.21824	0.00186	40.7	4.148×10^{-05}	4.2000	11
5	1	4	1	91340.84780	0.00173	20.0	4.741×10^{-05}	4.8000	11
5	0	4	0	91342.72461	0.00189	13.2	4.939×10^{-05}	5.0000	11
6	5	5	5	109553.96919	0.01021	190.5	2.644×10^{-05}	1.8333	13
6	4	5	4	109574.20539	0.00662	128.6	4.810×10^{-05}	3.3333	13
6	3	5	3	109589.95432	0.00384	80.4	6.496×10^{-05}	9.0000	26
6	2	5	2	109601.20873	0.00219	46.0	7.701×10^{-05}	5.3333	13
6	1	5	1	109607.96344	0.00203	25.3	8.425×10^{-05}	5.8333	13
6	0	5	0	109610.21536	0.00223	18.4	8.666×10^{-05}	6.0000	13
7	6	6	6	127782.68995	0.01698	272.3	3.683×10^{-05}	3.7143	30
7	5	6	5	127811.51930	0.01162	196.6	6.805×10^{-05}	3.4286	15
7	4	6	4	127835.12506	0.00755	134.7	9.361×10^{-05}	4.7143	15
7	3	6	3	127853.49637	0.00439	86.5	1.135×10^{-04}	11.4286	30
7	2	6	2	127866.62477	0.00249	52.1	1.278×10^{-04}	6.4286	15
7	1	6	1	127874.50422	0.00232	31.4	1.363×10^{-04}	6.8571	15
7	0	6	0	127877.13111	0.00254	24.5	1.391×10^{-04}	7.0000	15

Notes.
(*) The entire table is electronically available at the CDS via anonymous ftp to cdsarc.u-strasbg.fr (130.79.128.5) or via http://cdsweb.u-strasbg.fr/cgi-bin/qcat?J/A+A
(a) Upper and lower J_K quantum numbers.
(b) Predicted frequency (in MHz).
(c) Uncertainty in the predicted frequency (in MHz).
(d) Energy (in K) of the upper energy level of the transition.
(e) Einstein coefficient of the transition (in s^{-1}).
(f) Line strength.
(g) Degeneracy of the upper level. It is $2J+1$ for all levels except for those with $K=3\times$ n (n=1,2,...), for which g_u is $2\times(2J+1)$.